Opto-Ultrasonic Communications in Wireless Body Area Nanonetworks

G. Enrico Santagati and Tommaso Melodia
University at Buffalo, The State University of New York
Buffalo, NY, USA
Email: {santagat, tmelodia}@buffalo.edu

***Abstract*—Wirelessly interconnected nanorobots, i.e., engineered devices of sizes ranging from one to a few hundred nanometers, are promising revolutionary diagnostic and therapeutic medical applications that could enhance the treatment of major diseases. Each nanorobot is usually designed to perform a set of basic tasks such as sensing and actuation. A dense wireless network of nano-devices, i.e., a nanonetwork, could potentially accomplish new and more complex functionalities, e.g., in-vivo monitoring or adaptive drug-delivery, thus enabling revolutionary nanomedicine applications.**

Several innovative communication paradigms to enable nanonetworks have been proposed in the last few years, including electromagnetic communications in the terahertz band, or molecular and neural communications. In this paper, we propose and discuss an alternative approach based on establishing intra-body opto-ultrasonic communications among nanorobots. Opto-ultrasonic communications are based on the optoacoustic effect, which enables the generation of high-frequency acoustic waves by irradiating the medium with electromagnetic energy in the optical frequency range. We first discuss the fundamentals of nanoscale opto-ultrasonic communications in biological tissues, and then we model the generation, propagation, and detection of opto-ultrasonic waves.

I. Introduction

Wirelessly interconnected nanorobots, i.e., devices of sizes ranging from one to a few hundred nanometers, are a promising solution for remote and distributed medical diagnosis and treatment of major diseases [1]. Each nanorobot is usually designed to perform a set of basic tasks such as sensing and actuation. A dense wireless interconnection of nanodevices, i.e., a nanonetwork, could potentially accomplish new and more complex functionalities, e.g., in-vivo monitoring or adaptive drug-delivery, thus enabling revolutionary nano-medicine applications. Nano-sensors and nano-actuators distributed in the human body could enable pervasive and reactive continuous in-vivo monitoring. Furthermore, wirelessly controlled nanorobots may be used to detect and eliminate malicious agents and cells inside biological tissues, e.g., viruses and cancer cells, enabling less invasive and less aggressive treatments [2]. Moreover, networked nano-devices could be used for organ, nervous track, or tissue replacements, i.e., bio-hybrid implants.

Several innovative communication paradigms have been proposed during the last few years, including terahertz band communications [3], or molecular and neural communications [4], [5]. In this paper, we take a different approach and investigate and study the use of ultrasonic waves to enable wireless networking between intra-body nanorobots.

Acoustic waves are known to propagate better than their radio frequency (RF) counterpart in media composed mainly of water and have been used successfully for underwater communications [6], and for ultrasonic imaging [7]. In [8], [9], we showed that ultrasonic waves have a strong potential to enable internetworking among devices implanted in the human body at communication ranges spanning from few μm to several cm; while in [10] the authors, based on consideration on the physics of ultrasound propagation, investigate the power requirements for acoustic communications between nanorobots across various distances and tissues. However, as of today and to best of our knowledge, no existing studies have explored the feasibility of ultrasonic wave generation and detection at the nanoscale for communication purposes.

Ultrasounds are typically generated through *piezoelectric* materials that convert electrical energy into mechanical energy and vice versa; or through the vibration of a thin plate, i.e., a capacitor, under *electrostatic* forces. Microelectro-mechanical system (MEMS) technology enables the fabrication of both microscopic piezoelectric and electrostatic ultrasonic transducers [11]. However, microscopic transducers do not satisfy the size requirements for being embedded into devices with nanoscopic dimensions. While, to best of our knowledge, no reports of nanoelectro-mechanical system (NEMS) ultrasonic transducers have appeared in the literature yet, initial successful attempts at developing nano-ultrasonic transducers based on the optoacoustic effect [12] have been reported.

The optoacoustic effect refers to the generation of acoustic waves from the optical excitation of a medium. In optoacoustics, acoustic waves can be generated through various mechanisms, including optical breakdown, vaporization, and thermoelastic generation. In this paper, we consider the thermoelastic mechanism, where the energy irradiated by a laser is absorbed by the tissue surface or by an intermediate material causing rapid heating, and thus thermoelastic expansion, which in turn generates ultrasonic waves. Faster transient heating generates higher frequency components. For example, optical pulses a few nanoseconds long can generate ultrasonic pulses with central frequency and bandwidth in the order of hundreds of MHz. We refer to ultrasonic waves generated through optical sources as opto-ultrasonic waves.

The joint use of light beams and ultrasonic waves that characterizes optoacoustics could potentially be the foundation of a new communication paradigm to enable intra-body networking at the nanoscale. In fact, EM waves in the optical frequency range do not propagate easily in tissues; while ultrasonic waves propagate fairly well in media composed mainly of water. At the same time, generating and detecting ultrasounds through pulsed lasers has several advantages with respect to

traditional piezoelectric and capacitive ultrasonic transducers, i.e., higher miniaturization, higher bandwidth and higher sensitivity [12]. Finally, recent advances in nano-optics have made the design and fabrication of nanoscopic optical sources, i.e., nanolasers, possible [13]. However, photoacoustic generation of ultrasounds also introduces significant challenges that need to be addressed to enable the design of transmission schemes and networking protocols for intra-body nanonetworks.

In this paper, we discuss the fundamentals of nanoscale opto-ultrasonic communications in biological tissues. In Section II we discuss the potential hazards posed by using opto-ultrasonic communications in the human body. In Section III, IV, and V, we model opto-ultrasonic wave generation, propagation, and detection, respectively. Finally, in Section VI we conclude the paper.

II. Opto-Ultrasonic Waves and Health Concerns

Optical Bioeffects. Opto-ultrasonic waves are generated through various optoacoustic mechanisms, such as optical breakdown, vaporization and thermoelastic generation. Optical breakdown and vaporization present high generation efficiency, i.e., the ratio between the acoustic energy generated over the optical energy absorbed, but they require extremely high laser intensities that may produce detrimental and irreversible effects in the radiated tissue. Instead, the thermoelastic mechanism has lower generation efficiency, but requires significantly lower laser intensities compared to the optical breakdown and vaporization effects. This mechanism is in general more attractive because of its non-destructive and low-thermal effect properties.

Since nanorobot communications need to be non-destructive we focus on thermoelastic generation only. Thus, in the rest of this paper, we assume that optical excitation energies are lower than the breakdown and vaporization thresholds. Moreover, we assume that the excitation energy is lower than a safety threshold given by the maximum permissible exposure (MPE) recommendations defined by the American National Standards Institute (ANSI) [14]. The ANSI standard defines formulas to determine the *repetitive excitation* MPE for different wavelength ranges, pulse repetition frequencies, and single-pulse durations.

Acoustic Bioeffects. The most well-understood acoustic effect in biological tissues is *heating*. During ultrasound propagation, a portion of the energy is absorbed and converted into heat, which could lead to a temperature increase. As the wave intensity increases, the temperature rises and if it becomes higher than $38.5°C$, adverse biological effects may occur. Another effect caused by ultrasonic wave propagation is *cavitation*, which denotes the behavior of gas bubbles within an acoustic field. Pressure variations of the ultrasound wave cause bubbles in the propagation medium to contract and expand. For large pressure variations, the bubble may collapse, causing serious biological effects and damaging tissues located in close proximity. High-frequency and impulsive transmissions can potentially reduce both heating and cavitation effects.

Ultrasounds have been successfully used for therapeutic and diagnostic purposes inside the human body since the 1960s with no detrimental effects. The medical experience of the last decades has demonstrated that ultrasound is fundamentally *safe*, as long as tissues are exposed to acoustic intensities below $10^3\ \mathrm{pW}/\mu\mathrm{m}^2$ for unfocused ultrasounds [15]. In general, detrimental effects have not been observed when the acoustic energy imparted to the tissue, i.e., the product of intensity and exposure time, is less than 50 J/cm^2 [15], [8]. Therefore, ultrasounds at low transmission pressure levels, and consequently low transmission power levels, are known to not cause any lethal bioeffects. Therefore, opto-ultrasonic communications can be a safe and reliable alternative to classical electromagnetic RF communications.

III. Opto-ultrasonic wave generation

Thermoelastic Generation Model. Assume a stationary and non-viscous soft-tissue with negligible thermal conductivity, as well as the linear acoustic approximation and absence of absorption. Under these conditions, if sound speed and density are constant in space, the acoustic pressure as a function of time t and of the three-dimensional space vector $\mathbf{r}$, $P(\mathbf{r},t)$ [Pa], obeys the acoustic wave equation [16],

$$\frac{\partial^2 P(\mathbf{r},t)}{\partial t^2} - c^2\nabla^2 P(\mathbf{r},t) = \Gamma\frac{\partial \mathcal{H}(\mathbf{r},t)}{\partial t}, \tag{1}$$

where c [m/s] is the speed of sound, $\Gamma = \frac{\beta c^2}{C_p}$ is the dimensionless Grüneisen coefficient, which measures the conversion efficiency from optical energy to pressure, β [K^{-1}] is the thermal volume expansion coefficient, C_p [$\mathrm{J\,kg^{-1}K^{-1}}$] is the specific heat capacity of the medium, and $\mathcal{H}(\mathbf{r},t)$ [$\mathrm{J\,m^{-3}s^{-1}}$] is the heat energy absorbed by the tissue per unit time and unit volume. If we assume the source to be stationary, the heating component can be written as $\mathcal{H}(\mathbf{r},t) = E_a G(\mathbf{r})T(t)$, where $T(t)$ [s^{-1}] and $G(\mathbf{r})$ [m^{-3}] represent the temporal profile and the radial profile of the heat source, respectively, and are related to the radiating source, i.e., the beam diameter and the duration of the pulses. The term E_a [J] represents the total energy absorbed by the tissue. If the excitation is caused by a very short optical pulse, the absorbed heat becomes $\mathcal{H}(\mathbf{r},t) = E_a G(\mathbf{r})\delta(t)$, where $\delta(t)$ is the *Dirac* function. A solution to (1), under the very-short excitation assumption, represents the evolution of the pressure field in time and space for an ideal instantaneous radiation. The solution for a finite, hence real, pulse can be found by calculating the convolution between the ideal solution and the temporal laser pulse profile [17]. Specifically, let us assume a spherical Gaussian radial and temporal profile for the source. Under this assumption the radial profile $G(\mathbf{r})$ depends only on the radial component of the vector $\mathbf{r}$, i.e., its Euclidean norm, that we denote as r. Under far-field condition ($r \gg R$), we obtain the following generated pressure field [18]

$$P(r,t) = -\frac{\beta E_a}{2(2\pi)^{3/2}C_p r}\frac{t-\tau}{\tau_e^3}e^{-\frac{1}{2}\left(\frac{t-\tau}{\tau_e}\right)^2}, \tag{2}$$

where R is the radius of the source sphere, τ_l is the characteristic width of the temporal profile[1], $\tau = \frac{r}{c}$, $\tau_a = \frac{R}{c}$ and $\tau_e = \sqrt{\tau_a^2 + \tau_l^2}$ is the effective characteristic width of the optoacoustic temporal profile. According to this model, τ_e depends on both the *duration* of the optical pulse and

[1]Half the pulse duration between the 1/e-points of the temporal amplitude distribution.

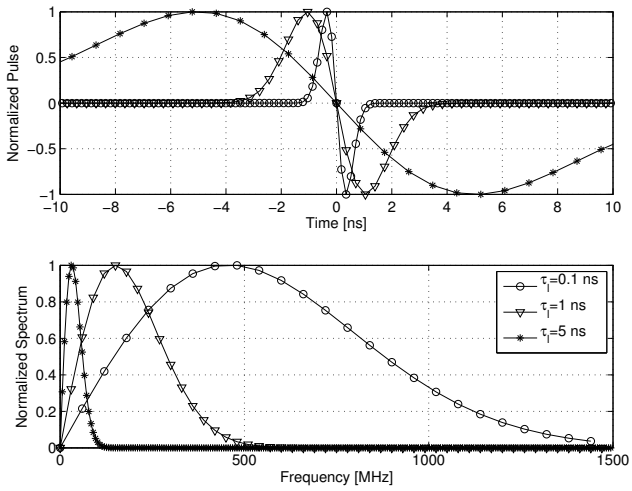

Fig. 1. Normalized temporal profile and normalized spectrum of the generated opto-ultrasonic pulse for different characteristic widths of the temporal profile τ_l and with sphere radius $R = 500\,\mathrm{nm}$.

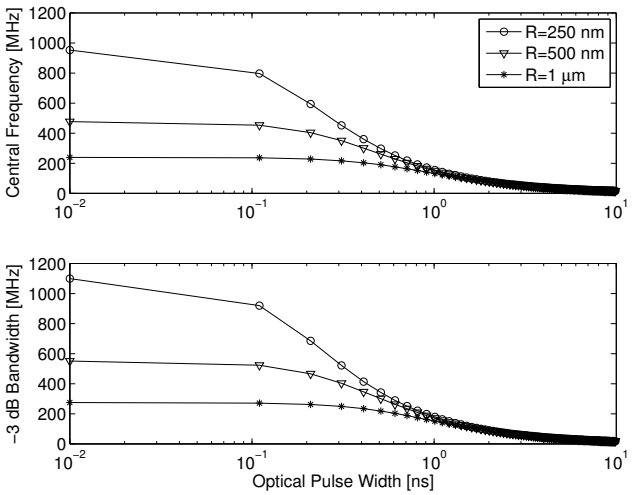

Fig. 2. Central frequency and -3 dB bandwidth of the generated opto-acoustic signal as a function of τ_l for three different values of the sphere radius R.

on the *width* of the optical beam. We also observe that the amplitude of the generated pulse depends linearly on the thermal expansion coefficient β and on the total energy absorbed E_a. The optical excitation source must be tuned based on these observations to operate at desired frequency and acoustic intensity ranges.

Opto-Ultrasonic Frequency Spectrum. We now show how the opto-ultrasonic signal frequency spectrum depends on the optical pulse duration and on the optical beam width. By Fourier-transforming (2), we obtain the amplitude spectrum of the generated signal [18]

$$|P(r,f)| = \frac{\beta E_a}{2C_p r} f e^{-2(\pi\tau_e f)^2}. \tag{3}$$

Figure 1 shows the normalized temporal profile and the normalized spectrum of the generated opto-ultrasonic pulse when varying the optical pulse duration, i.e., for different characteristic widths of the temporal profile τ_l, assuming a sphere radius R of $500\,\mathrm{nm}$, corresponding to the radiating surface of a potential nanolaser. We observe that shorter optical pulses have higher central frequency and a larger bandwidth. For example, with a $5\mathrm{ns}$-long optical pulse, we obtain an opto-ultrasonic signal with central frequency of $150\,\mathrm{MHz}$ and about $170\,\mathrm{MHz}$ of $-3\mathrm{dB}$ bandwidth. In Fig. 2, the central frequency and the $-3\mathrm{dB}$ bandwidth of the generated opto-acoustic signal is plotted as a function of τ_l, for three different values of the sphere radius R. We observe that, according to the sphere dimensions, when $\tau_l < \tau_a$, both the central frequency and the $-3\,\mathrm{dB}$ bandwidth are strongly dependent on the sphere radius, but less dependent on the optical pulse duration. Instead, when the pulse duration becomes such that $\tau_l > \tau_a$, the opto-ultrasonic signal spectrum becomes independent of the beam radius and it only depends on the optical pulse duration. Therefore, for a given beam radius R, which depends on the nanorobot dimensions and the size of the optical source, there is a maximum frequency limit that cannot be overcome even by further reducing the optical pulse duration. For example, for a $500\,\mathrm{nm}$-radius optical beam, the maximum achievable central frequency is about $500\,\mathrm{MHz}$.

IV. Opto-Ultrasonic Wave Propagation in Tissues

Attenuation. Two main mechanisms contribute to ultrasound attenuation in tissues, i.e., absorption and scattering. An initial pressure P_0 decays at a distance r according to [19]

$$P(r) = P_0 e^{-\alpha r}, \tag{4}$$

where α (in $[\mathrm{Np\ cm^{-1}}]$) is an amplitude attenuation coefficient that captures all the effects that cause dissipation of energy from the ultrasonic wave. Parameter α depends on the carrier frequency through $\alpha = af^b$, where f represents the carrier frequency (in MHz) and a (in $[\mathrm{Np\ cm^{-1}\ MHz^{-b}}]$) and b are attenuation parameters characterizing the tissue [8]. In biological tissues, and for frequencies in the range of few MHz, b is approximately equal to 1. When the frequency range is higher than $10\mathrm{MHz}$, b has values close to 2, as in pure water. Therefore, the attenuation coefficient increases quadratically with frequency [10].

By multiplying (3) by the frequency-dependent sound absorption in (4), we obtain

$$|P(r,f)| = \frac{\beta E_a}{2C_p r} f e^{-[2(\pi\tau_e f)^2 + raf^b]}. \tag{5}$$

If we assume to operate at frequencies greater than $10\,\mathrm{MHz}$, where $b = 2$, we can Fourier-invert (5) and obtain the opto-ultrasonic field $P(r,t)$ in the presence of absorption. As a result, $P(r,t)$ is still described by (2), with the exception that the effective time constant is now $\tau_e'(r) = \sqrt{\tau_a^2 + \tau_l^2 + \frac{ra}{2\pi^2}}$. However, for short-range communications, i.e., $ra < \tau_e$, the absorption effect in (4) is relatively small when compared with the pressure decrease caused by the spreading of the acoustic wave. Under this condition, the initial pressure P_0 decreases in an inversely proportional way with respect to the distance r from the source [18].

Propagation Delay. The propagation speed of acoustic waves in biological tissues is approximately $1500\,\mathrm{m/s}$, with a small variation of less than 10% in most soft tissues, as compared to $2 \times 10^8\,\mathrm{m/s}$ [20] for RF waves. However, for the relatively short communication ranges considered, i.e., in the

order of a few hundreds of μm, the propagation delay is in the order of tens of nanoseconds. Moreover, since the internal body temperature is subject to relatively small variations, i.e., a few $^{\circ}\mathrm{C}$, the temperature dependence of the speed of sound can be usually neglected for ultrasonic propagation in tissues.

Reflections and Scattering. The human body is composed of different organs and tissues with different sizes, densities and sound speeds. Therefore, it can be modeled as an environment with pervasive presence of *reflectors* and *scatterers*. The direction and magnitude of the reflected wave depend on the orientation of the boundary surface and on the acoustic impedance of the tissues, Z, measured in Rayl [$\mathrm{kg\ s^{-1}\ m^{-2}}$] [8]. Scattered reflections occur when an acoustic wave encounters an object that is relatively small with respect to its wavelength or a tissue with an irregular surface. Consequently, the received signal is obtained as the sum of numerous attenuated, possibly distorted, and delayed versions of the transmitted signal.

Operating Frequency. Several key aspects need to be considered to determine an optimal operating frequency for intra-body opto-ultrasonic communications. Specifically, (i) the *attenuation coefficient* increases with frequency; (ii) the *beam spread* of the generated ultrasonic waves is inversely proportional to the ratio of the diameter of the radiating element and the wavelength [8]; (iii) the *ultrasonic power efficiency*, defined as the fraction of excitation power that produces acoustic radiation (and is not dissipated against viscous forces), increases with frequency [10]; finally, (iv) the *maximum achievable frequency* of the optoacoustic source is limited by its size, as discussed in Section III. Therefore, one needs to operate at frequencies corresponding to the desired compromise between beam directivity and ultrasonic power efficiency, and that are at the same time compatible with the source dimension and the maximum tolerable attenuation.

In [8] we observed that, given the limited attenuation effect due to absorption in short-range communications, the operating frequency may be as high as $1\ \mathrm{GHz}$. In [10], the authors observed that for a $500\ \mathrm{nm}$-radius nanorobot the transmission efficiency, i.e., the fraction of emitted power that reaches a distance of $100\ \mu\mathrm{m}$, which depends on both the attenuation and the ultrasonic power efficiency, has a maximum around $150\,\mathrm{MHz}$. Finally, as reported in Section III, the maximum achievable central frequency for a $500\ \mathrm{nm}$-radium opto-ultrasonic source is approximately $500\,\mathrm{MHz}$. Therefore, in accordance with our previous results in [8], we expect that nanorobots communicating over short-range distances, i.e., less than a mm, will be able to successfully operate at frequencies in the order of a few hundreds of MHz.

V. Opto-ultrasonic wave detection

Optical detection of ultrasounds is based on measuring the variations induced by the acoustic field on a target optical field. Specifically, by using an optical resonator, an arrangement of mirrors that creates a standing wave cavity resonator for light waves [21], the interaction between the optical and acoustic fields takes place in a resonant cavity. As a result, the incident beam goes through several reflections in the resonant cavity, each time producing a reflected signal, i.e., a signal emitted in the direction opposite to the incident beam direction, whose intensity depends on the optical path length within the resonator. The displacement produced by the incident acoustic wave changes the cavity length, and hence modulates the intensity of the reflected signal [22].

An optical resonator can be modeled as a Fabry-Pérot interferometer, also known as an *etalon* [23]. Given an incident light intensity I_0 [$\mathrm{W\ m^{-2}}$], the reflected beam intensity is the complementary of the transmitted beam intensity, i.e., $I_r + I_t = I_0$, and can be expressed as

$$I_r = I_0 \left(1 - \frac{1}{1 + K \sin^2(\Phi/2)}\right). \tag{6}$$

The quantity Φ [rad] is the round trip phase shift and is expressed as $\Phi = \frac{4\pi n L \nu}{c}$, where L [m] is the resonator length, n is the index of refraction of the etalon material, c [m/s] is the speed of light, and ν [Hz] is the optical frequency. The coefficient K is given by $K = \frac{4R}{(1-R)^2}$, where R is the reflectivity of the resonator mirrors.

Receiver Sensitivity. Using a first order approximation, for a small change in length δL, i.e., a small ultrasonic pressure reaching the receiver surface, the reflected light intensity variation is given by [22]

$$\delta I_R = I_0 \frac{9}{2\sqrt{3}} \left(\frac{\mathcal{F} c \delta L}{\lambda}\right), \tag{7}$$

where $\mathcal{F}$ is the cavity finesse, defined as $\mathcal{F} = \frac{\pi}{2}\sqrt{K}$. We can observe that a higher finesse results in higher ultrasonic detection sensitivity. Finally, the receiver acoustic sensitivity, i.e., the minimum pressure detectable by the receiver, can be expressed as [22]

$$S_r = \sqrt{\frac{4qB}{27 S I_0}} \left(\frac{\lambda}{\mathcal{F} n}\right) \frac{Y}{L}, \tag{8}$$

where S [A/W] is the optical detector sensitivity, q [C] is the electron charge, and B [Hz] is the detection bandwidth of the photodetector. Y [Pa] represents the Young's modulus of the etalon, which establishes the relationship between the etalon deformation and the corresponding pressure. We observe that the sensitivity of the receiver increases with higher finesse or with longer cavity. Moreover, the finesse depends only on the mirror reflectivity, and not on the cavity length. Therefore, the receiver sensitivity can be adjusted by independently tuning either the finesse or the cavity length. Another advantage is that the sensitivity does not depend on the dimension of the active area, defined by the diameter of the probing optical beam. Therefore, very small aperture and wideband ultrasound receivers still have high sensitivity, thus overcoming the limitations of piezoelectric transducers, whose sensitivity decreases with the element size [24].

Receiver Bandwidth. The receiver bandwidth is determined by the frequency response of the cavity, which is obtained by considering the distribution of stress across the thickness of the cavity caused by an incident acoustic wave [25],

$$|C(f)| \propto \frac{1}{f} \frac{\left|\left(e^{i\frac{2\pi f}{c}L} - 1\right) + R_1\left(1 - e^{-i\frac{2\pi f}{c}L}\right)\right|}{\left|1 - R_1 R_2 e^{-i\frac{2\pi f}{c}2L}\right|}, \tag{9}$$

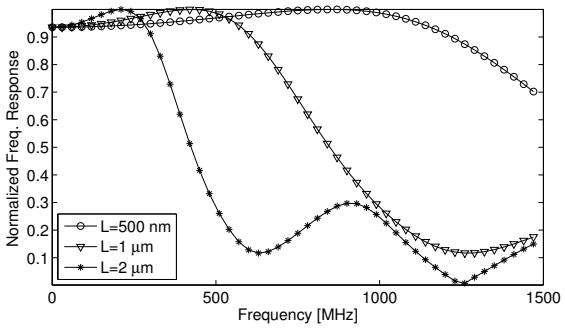

Fig. 3. Normalized frequency response of an etalon-based opto-ultrasonic detector.

where L is the thickness of the cavity, and c is the speed of sound in the etalon material. R_0 and R_1 represent the acoustic reflection coefficient due to the acoustic impedance mismatch between the external medium, e.g., a biological tissue, and the etalon material, and between the etalon material and the backing material, respectively. The acoustic reflection coefficient depends on the acoustic impedances of the two materials in the interface, Z_1 and Z_2, as $R = \frac{Z_1 - Z_2}{Z_1 + Z_2}$. Figure 3 shows the normalized frequency response of the etalon-based opto-ultrasonic detector for three different cavity lengths, assuming the external tissue to be skeletal muscle, the backing material to be glass, and the cavity material to be SU-8 photoresist, a polymer commonly used in the microelectronics industry [25]. We observe that, by reducing the cavity length, the frequency response of the opto-ultrasonic detector shifts towards higher frequencies, thus offering significantly larger bandwidth. For example, by reducing the cavity length of the detector from $2\,\mu\mathrm{m}$ to $500\,\mathrm{nm}$, the $-3\,\mathrm{dB}$ bandwidth increases from approximately $400\,\mathrm{MHz}$ to more than $1\,\mathrm{GHz}$.

VI. Conclusions

We explored some fundamental aspects of nanoscale opto-ultrasonic communications in biological tissues. We first discussed the potential hazards of using opto-ultrasonic communications in the human body. Then, we modeled the generation, propagation, and detection of opto-ultrasonic waves. Finally, we discussed tradeoffs such as the choice of an optimal transmission frequency and dependence of the bandwidth on the optical source size and on the optical excitation duration.

Acknowledgements

This work is based on material supported by the US National Science Foundation under grant CNS-1253309.

References

[1] I. F. Akyildiz, F. Brunetti, and C. Blázquez, "Nanonetworks: A new communication paradigm," *Comput. Netw.*, vol. 52, no. 12, pp. 2260–2279, Aug. 2008.

[2] J. Baker, A. Quintana, L. Piehler, M. Banazak-Holl, D. Tomalia, and E. Raczka, "The synthesis and testing of anti-cancer therapeutic nanodevices," *Biomedical Microdevices*, vol. 3, no. 1, pp. 61–69, 2001.

[3] I. F. Akyildiz and J. M. Jornet, "Electromagnetic wireless nanosensor networks," *Nano Communication Networks*, vol. 1, no. 1, pp. 3–19, Mar. 2010.

[4] M. Pierobon and I. Akyildiz, "A physical end-to-end model for molecular communication in nanonetworks," *Selected Areas in Communications, IEEE Journal on*, vol. 28, no. 4, pp. 602–611, 2010.

[5] L. Galluccio, S. Palazzo, and G. E. Santagati, "Characterization of molecular communications among implantable biomedical neuro-inspired nanodevices," *Nano Communication Networks*, vol. 4, no. 2, pp. 53 – 64, 2013.

[6] T. Melodia, H. Kulhandjian, L. Kuo, and E. Demirors, "Advances in Underwater Acoustic Networking," in *Mobile Ad Hoc Networking: Cutting Edge Directions*, second edition ed., S. Basagni, M. Conti, S. Giordano, and I. Stojmenovic, Eds. Inc., Hoboken, NJ: John Wiley and Sons, 2013, pp. 804–852.

[7] F.L. Thurstone, H.E. Melton, "Biomedical Ultrasonics," *IEEE Trans. on Ind. Electr. and Contr. Instrum.,*, vol. 17, no. 2, Apr. 1970.

[8] L. Galluccio, T. Melodia, S. Palazzo, and G. E. Santagati, "Challenges and Implications of Using Ultrasonic Communications in Intra-body Area Networks," in *Proc. of IEEE Intl. Conf. on Wireless On-demand Networked Systems (WONS)*, Courmayeur, Italy, Jan. 2012.

[9] G. E. Santagati, T. Melodia, L. Galluccio, and S. Palazzo, "Distributed MAC and Rate Adaptation for Ultrasonically Networked Implantable Sensors," in *Proc. of IEEE Conf. on Sensor, Mesh and Ad Hoc Communications and Networks (SECON)*, New Orleans, LA, June 2013.

[10] T. Hogg and R. A. Freitas, "Acoustic Communication for Medical Nanorobots," *Nano Communication Networks (Elsevier)*, vol. 3, no. 2, pp. 83–102, Feb. 2012.

[11] M. Pappalardo, G. Caliano, A. Savoia, and A. Caronti, "Micromachined ultrasonic transducers," in *Piezoelectric and Acoustic Materials for Transducer Applications*, A. Safari and E. Akdoan, Eds. Springer US, 2008, pp. 453–478.

[12] R. Smith, A. Arca, X. Chen, L. Marques, M. Clark, J. Aylott, and M. Somekh, "Design and fabrication of nanoscale ultrasonic transducers," *Journal of Physics: Conference Series*, vol. 353, no. 1, 2012.

[13] J. Y. Suh, C. H. Kim, W. Zhou, M. D. Huntington, D. T. Co, M. R. Wasielewski, and T. W. Odom, "Plasmonic bowtie nanolaser arrays," *Nano Letters*, vol. 12, no. 11, pp. 5769–5774, 2012.

[14] A. N. S. Institute and L. I. of America, *American National Standard for Safe Use of Lasers in Health Care Facilities: Standard Z136.1-2000*. New York: ANSI, Inc., 2000.

[15] D. L. Miller, "Safety assurance in obstetrical ultrasound," *Seminars in Ultrasound, CT and MRI*, vol. 29, no. 2, pp. 156 – 164, 2008, ¡ce:title¿Ultrasound in Obstetrics and Gynecology¡/ce:title¿.

[16] B. T. Cox, S. Kara, S. R. Arridge, and P. C. Beard, "k-space propagation models for acoustically heterogeneous media: Application to biomedical photoacoustics," *Acoustical Society of America*, vol. 121, no. 6, Feb. 2007.

[17] G. B. Arfken, H. J. Weber, and F. E. Harris, *Mathematical Methods for Physicists, Sixth Edition: A Comprehensive Guide*, 6th ed. Academic Press, Jul. 2005.

[18] C. G. A. Hoelen and F. F. M. de Mul, "A new theoretical approach to photoacoustic signal generation," *The Journal of the Acoustical Society of America*, vol. 106, no. 2, pp. 695–706, 1999.

[19] C. R. Hill, *Ultrasonic attenuation and scattering by tissues*. John Wiley & Sons, Inc., 1978.

[20] F. P. Bolin, L. E. Preuss, R. C. Taylor, and R. J. Ference, "Refractive index of some mammalian tissues using a fiber optic cladding method," *Appl. Opt.*, vol. 28, no. 12, pp. 2297–2303, Jun 1989.

[21] N. Hodgson and H. Weber, *Optical Resonators: Fundamentals, Advanced Concepts, Applications*, ser. Springer Series in Optical Sciences. Springer, 2005.

[22] J. Hamilton, T. Buma, M. Spisar, and M. O'Donnell, "High frequency optoacoustic arrays using etalon detection," *Ultrasonics, Ferroelectrics and Frequency Control, IEEE Transactions on*, vol. 47, no. 1, pp. 160–169, Jan.

[23] G. Hernandez, *Fabry-Pérot Interferometers*, ser. African Studies Series. Cambridge UniversityPress, 1986.

[24] V. Wilkens, "Characterization of an optical multilayer hydrophone with constant frequency response in the range from 1 to 75 mhz," *The Journal of the Acoustical Society of America*, vol. 113, no. 3, pp. 1431–1438, 2003.

[25] Y. Hou, S.-W. Huang, R. Witte, M. O'Donnell, and S. Ashkenazi, "Thin polymer etalon arrays for high-resolution photoacoustic imaging," *Journal of Biomedical Optics*, vol. 13, no. 6, pp. 064 033–064 033–8, 2008.